THE ASTROPHYSICAL JOURNAL, 459:193–208, 1996 March 1

THE NATURE OF THE RADIO SOURCES WITHIN THE CEPHEUS A STAR-FORMING REGION

GUIDO GARAY,[1] SOLANGE RAMÍREZ,[1] LUIS F. RODRÍGUEZ,[2] SALVADOR CURIEL,[3] AND JOSÉ M. TORRELLES[4]
Received 1995 February 7; accepted 1995 September 7

ABSTRACT

We present multifrequency, matching-beam, VLA radio continuum observations of the Cep A East radio source, known to consist of 16 compact ($\sim 1''$) components clustered within a 25″ radius region, most of which are aligned in stringlike structures. We find that the spectral indices of the emission from these compact objects, in the frequency interval from 1.5 to 15 GHz, cover a wide range, from -0.6 to 0.7. Positive spectral indices are exhibited by sources 2, 3b, 3c, and 3d. The first and last of these objects, the brightest sources within Cep A East, exhibit in addition elongated morphologies and angular-size and flux-density dependences with frequency that suggest they correspond to confined jets of ionized gas.

Most of the objects that appear in string structures exhibit a mixture of flat and negative spectral indices across their faces, which indicates the presence of both thermal and nonthermal emission. The spectral indices of the integrated emission from sources 1b, 4, 6, and 7a are in the range between -0.3 and -0.1 while those of sources 1a, 5, 7b, and 7c are even more negative ($-0.6 \leq \alpha \leq -0.4$). We suggest that the radio emission from the string sources arises in shocks resulting from the interaction of confined stellar winds with the surrounding medium. The duality in emission mechanisms is expected in shock waves where a small fraction of the electrons are accelerated to relativistic velocities, giving rise to nonthermal emission, while most of the electrons produce thermal free-free emission. We find that the nonthermal emission dominates the thermal emission when the density of the thermal electrons is below a critical density of $\sim 5 \times 10^3$ cm^{-3}.

We also observed the Cep A West radio source, which consists of two compact components and an elongated, diffuse, champagne-like structure. We find that the spectral index between 1.5 and 5 GHz of the peak and of the integrated emission from the latter component are -0.1 and -0.4, respectively. We suggest that the radio emission from the diffuse source arises from shocked gas at the edge of a cavity driven by a wind that originates from the brightest compact radio object within this region, which shows a spectral index at the peak of the emission of 0.6.

Subject headings: H II regions — ISM: individual (Cepheus A) — ISM: jets and outflows — radio continuum: stars — stars: formation — stars: pre–main-sequence

1. INTRODUCTION

Cepheus A, located at a distance of 725 pc, is the densest condensation within the molecular cloud complex Cepheus OB3 (Sargent 1977). It has been identified as an active zone of star formation on the basis that it contains H_2O masers (Blitz & Lada 1979; Lada et al. 1981), OH masers (Rodríguez et al. 1980b; Cohen, Rowland, & Blair 1984), Herbig-Haro objects (Hartigan & Lada 1985; Lenzen 1988), IR sources (Lenzen 1988), and a bipolar outflow (Rodríguez, Ho, & Moran, 1980a; Bally & Lane 1990).

Two main regions of ionized gas, separated by $\sim 1'.5$, have been detected in Cepheus A: Cep A East and Cep A West (Hughes & Wouterloot 1982; Rodríguez & Cantó 1983). High-resolution radio continuum observations show that Cep A East consists of several compact sources, most of them appearing in stringlike structures. In their discovery observations, made with the VLA, Hughes & Wouterloot (1984) identified a total of 14 compact components. Later observations showed that some of these sources exhibited changes in their flux density and also revealed the presence of two new, highly variable, compact radio sources (Hughes 1988, 1991). Several of the compact radio sources are located at the edges of dense molecular clumps (Torrelles et al. 1985, 1986, 1993).

In spite of numerous studies made to date, a clear understanding of the nature of the radio emission from the Cep A East sources has not yet emerged. Hughes & Wouterloot (1984) and Hughes (1985) originally suggested that they represent very young, $\sim 10^3$ yr old, H II regions, each excited by a B3 star. This interpretation has, however, been questioned on several grounds (cf. Torrelles et al. 1986). For instance, it is difficult to explain how all the stars could be at about the same stage of evolution or why they were formed in lines. Alternatively, Torrelles and collaborators proposed that the radio continuum emission from the sources located at the edge of the molecular condensations arises from bright rims of ionized gas that are externally excited. They suggested as possible sources of heating and ionization the two bright, compact radio sources associated with H_2O maser emission (Cohen et al. 1984). Joyce & Simon (1986), on the other hand, suggested that the linear arrangements of H II regions correspond to shock-heated jets ejected from a young star.

Radio continuum observations at wavelengths of 20 and 6 cm with angular resolutions in the 0″.5–2″ range, made by

[1] Departamento de Astronomía, Universidad de Chile, Casilla 36-D, Santiago, Chile.
[2] Instituto de Astronomía–UNAM, Apdo. Postal 70-264, 04510 México D.F., Mexico.
[3] Harvard-Smithsonian Center for Astrophysics, 60 Garden Street, Cambridge, MA 02138.
[4] Instituto de Astrofísica de Andalucía, CSIC, Apdo. Correos 3004, CI Sancho Panza s/n, E-18080 Granada, Spain.

Hughes (1989), show that Cep A West consists of two compact objects seen toward the southeast and an extended, diffuse component located toward the northwest. The latter component is associated with a bright HH object that shows very broad Hα emission-line profiles of ~480 km s^{-1} (Hartigan et al. 1986). The line joining these three radio sources is directed toward the diffuse optical object GGD 37 (Gyulbudaghian, Glushkov, & Denisyuk 1978), identified as a group of HH objects (Hartigan & Lada 1985; Hartigan et al. 1986). There is no consensus on the driving source of the activity in this region. Lenzen (1988) concluded that the GGD 37 complex, as well as the HH object lying ~3.5 to the northeast from it (hereafter HH-NE), are shock-excited by the wind from a single star located at the center of the Cep A East region, possibly associated with the brightest radio source in that region. On the other hand, Hartigan & Lada (1985) suggested that Cep A West constitutes an independent region of activity, distinct from Cep A East. The source of energy was not identified, though.

In this paper we report new observations, made with the VLA, of the Cep A region that were designed to determine the spectral indices of the radio emission from its multiple components. Since some of them show extended envelopes and others are potentially variable, essential precepts in the determination of spectral indices are that the flux-density measurements must be made simultaneously and with the same angular resolution. Previous determinations of the spectral indices of these sources were made using data taken in different epochs and/or with different angular resolutions (Hughes & Wouterloot 1984; Hughes 1985). It is not known, however, how they are affected by variability and resolution. The purpose of our observations is twofold. First, knowledge of the spectral indices will permit the establishment of the nature of the radio emission; second, it will help to establish which of the compact radio sources are truly internally excited and hence to identify the powering sources of the activity within the Cep A region.

2. OBSERVATIONS

The observations were made with the Very Large Array of the National Radio Astronomy Observatory[5] during 1991 July 15 and 1991 December 13/14, with the array in the A and B configurations, respectively. To obtain angular resolutions of ~1″ at the different frequencies observed, we split the array into two subarrays. During the first observing session, with the array in the A configuration, we made matching-beam observations at 20 and 6 cm. The subarray used for the 20 cm observations consisted of the four outer antennas of each arm, which provided a range of spacings from 3.17 to 36.4 km. This range of spacings makes structures larger than ~13″ undetectable at 20 cm. The subarray used for the 6 cm observations was formed by the five inner antennas of each arm, which provided a range of spacings from 0.84 to 13.3 km. This range of spacings makes structures larger than ~15″ undetectable at 6 cm. The synthesized beams for maps made with natural weighting were 1.″07 × 1.″00 and 1.″02 × 1.″01 at 20 and 6 cm, respectively.

During the second observing session, with the array in the B configuration, we made matching-beam observations at 6 and 2 cm, designed to obtain images with angular resolutions similar to those in the first session and to check for source variability at 6 cm. The subarray used for the 6 cm observations consisted of the four outer antennas of each arm, which provided a range of spacings from 0.96 to 11.1 km. Structures larger than ~13″ are undetectable at 6 cm with these spacings. The subarray used for the 2 cm observations was formed by the five inner antennas of each arm, which provided a range of spacings from 0.26 to 4.0 km. This range of spacings makes structures larger than ~16″ undetectable at 2 cm. The synthesized beams for maps made with natural weighting were 1.″16 × 0.″78 and 1.″16 × 1.″15 at 6 and 2 cm, respectively.

The observations were made with an effective bandwidth of 100 MHz, which resulted from the use of two circular polarizers with 50 MHz bandwidth each. The phase center of the array was set at $\alpha(1950) = 22^h54^m19^s.04$, $\delta(1950) = 61°45'47''.4$. The flux-density scale was determined by observing 1328+307 (3C 286) while the phase calibrator was 0016+731. The data were edited and calibrated following the standard VLA procedures, using the Astronomical Image Processing System (AIPS). Maps were made by Fourier-transforming the (u, v) data with natural weighting and cleaned by use of the MX algorithm. Further, we applied a small Gaussian convolution in order that the beamwidth be exactly the same, 1.″2, at all frequencies. The observing dates, bands, central frequencies, configurations, angular resolutions, and the rms noise level in the maps are summarized in Table 1.

3. RESULTS

3.1. *Cep A East*

In Figure 1 we show the matching-beam maps, at the wavelengths of 20, 6, and 2 cm, of the Cep A East region. Comparison of our 6 cm map (*middle*) with the discovery map of Hughes & Wouterloot (1984), made at the same wavelength and with similar angular resolution, shows good agreement. To facilitate comparison we designate our sources (see bottom panel) with the same numbers and letters as those given by Hughes & Wouterloot (1984). The most obvious distinctions between these two maps are the difference in brightness of sources 3a and 9, the former being weaker and the latter being stronger at the times of

[5] The National Radio Astronomy Observatory is operated by Associated Universities, Inc., under cooperative agreement with the National Science Foundation.

TABLE 1

INSTRUMENTAL PARAMETERS

Observing Date	Band	Frequency (GHz)	Configuration	Synthesized Beam FWHM	Synthesized Beam P.A.	RMS Noise (mJy beam^{-1})
1991 Jul 15	L	1.49	A-outer	1.″07 × 1.″00	−7°	0.046
1991 Jul 15	C	4.86	A-inner	1.02 × 1.01	55	0.032
1991 Dec 13/14.....	C	4.86	B-outer	1.16 × 0.78	−74	0.027
1991 Dec 13/14.....	U	14.94	B-inner	1.16 × 1.15	−45	0.090

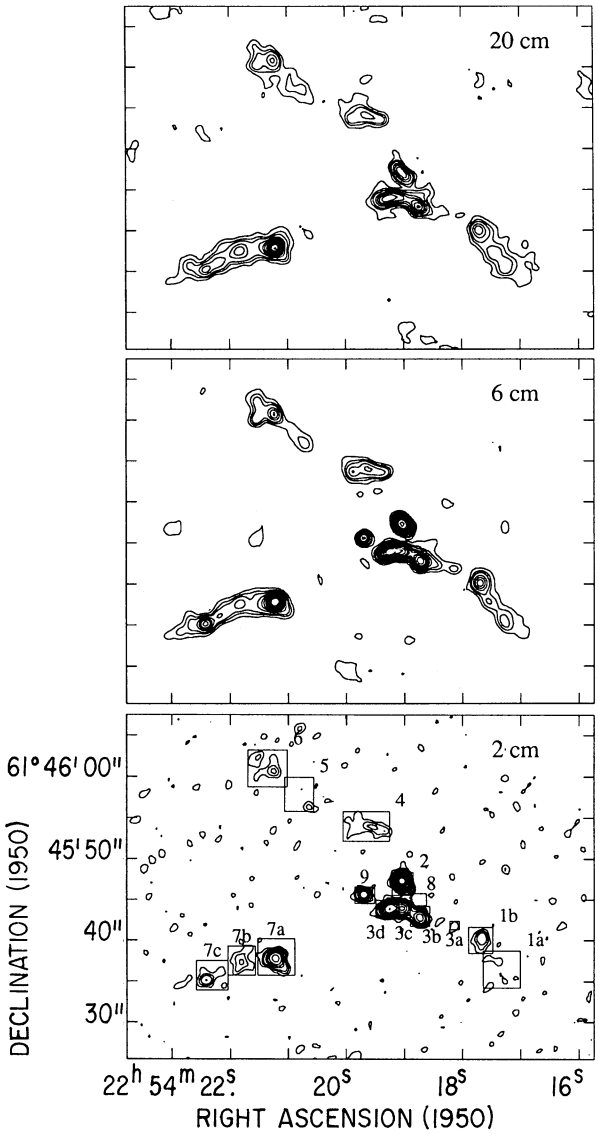

FIG. 1.—VLA radio continuum maps of the Cep A East region with 1".2 angular resolution. *Top*: 20 cm map. Contour levels are −1, 1, 2, 3, 5, 7, 9, 12, 15, 18, 22, and 26 × 0.15 mJy beam^{-1}. *Middle*: 6 cm map. Contour levels are −1, 1, 2, 3, 5, 7, 9, 12, 15, 20, 25, 30, 40, and 50 × 0.125 mJy beam^{-1}. *Bottom*: 2 cm map. Contour levels are −1, 1, 2, 3, 5, 7, 10, 15, 20, 30, 40, and 50 × 0.2 mJy beam^{-1}. The rectangles superposed on the 2 cm map correspond to the regions over which we added the flux densities per beam to obtain the integrated flux density.

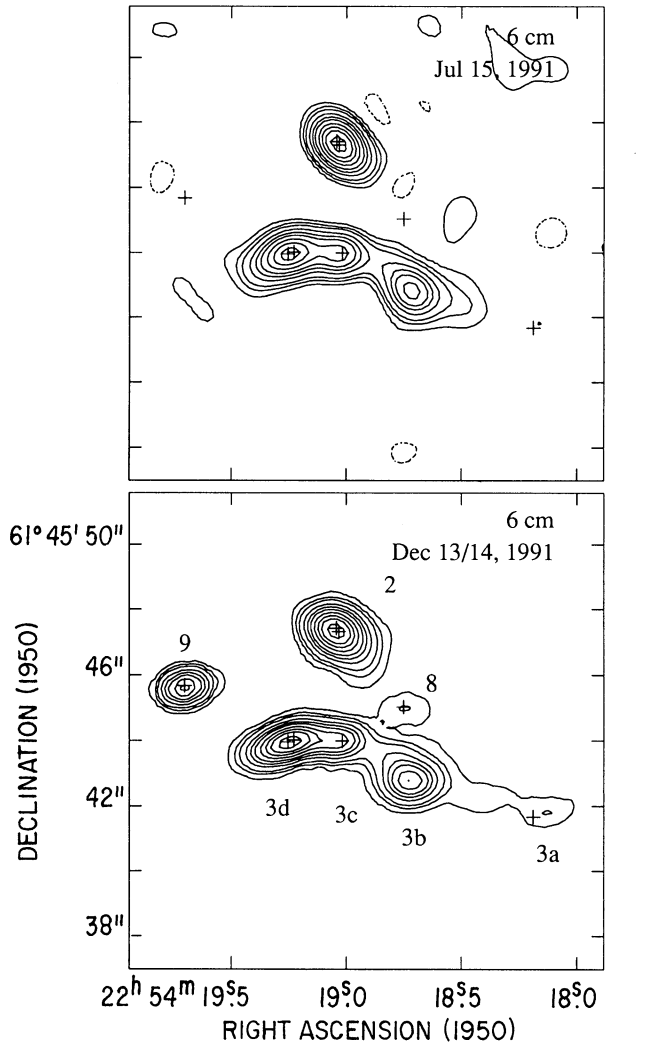

FIG. 2.—Comparison of 6 cm radio continuum maps of the central region of Cep A East obtained in 1991 July 15 (*top*) and 1991 December 13/14 (*bottom*). The angular resolution is 1".2. Contour levels are −1, 1, 2, 3, 5, 7, 9, 12, 15, 18, and 22 × 0.2 mJy beam^{-1}. Crosses mark the positions of the ultracompact radio sources reported by Hughes (1988).

our observations. Elliptical Gaussian fittings were made for all sources at all frequencies by use of the AIPS task IMFIT. Table 2 lists the positions, flux densities, and FWHM angular diameters of the sources we detected within the Cep A East region. The boxes shown in the lower panel of Figure 1 illustrate the areas used to compute the flux densities given in Table 2.

3.1.1. *Variability*

Maps of the 6 cm emission from the central region of Cep A East made from the observations carried out on 1991 July 15 and 1991 December 13/14 are shown in Figure 2. A comparison of these maps shows that sources 3a, 8, and 9 underwent appreciable changes in their flux densities. Source 9 is highly variable; its flux density was below the detection limits in 1991 July (<0.14 mJy) and increased to 3.0 mJy in 1991 December. Source 8 was detected in 1991 December with a flux density of 0.6 mJy but was undetected in 1991 July (<0.14 mJy). Source 3a was barely detected in 1991 July, having a flux density of ∼0.15 mJy, while it increased to 0.42 mJy in 1991 December. These three objects have already been established as variable sources (Hughes 1988, 1991). The flux densities of the remaining sources within the Cep A East region stayed constant in the interval of time between 1991 July and December (variations smaller than 5%). Consequently, spectral indices obtained for these sources (§ 3.1.3) are not affected by variability.

3.1.2. *Morphologies*

Our observations show that the radio objects that appear in stringlike structures (sources 1a, 1b, 4, 5, 6, 7a, 7b, 7c) exhibit irregular morphologies, characterized by the presence of relatively compact cores surrounded by halos of diffuse emission. We will refer to these objects as the *string sources*. The westerly string (hereafter string 1) consists of an elongated, diffuse, weak component toward the southwest (source 1a) and a comparatively compact component toward the northeast (source 1b). The full length of string 1 is ∼10", which at the distance of 725 pc corresponds to

TABLE 2

OBSERVED PARAMETERS OF CEPHEUS A EAST SOURCES

SOURCE	POSITION (1950) α	POSITION (1950) δ	FREQUENCY (GHz)	FLUX DENSITY (mJy)	ANGULAR SIZE[a]
Nonvariable Sources[b]					
1a	22h54m17s.27	61°45′35″.7	1.5	4.2 ± 0.2	2″.0
			4.9	2.2 ± 0.1	...
			14.9	1.1 ± 0.3	...
1b	22 54 17.68	61 45 40.0	1.5	3.2 ± 0.1	1.6
			4.9	2.9 ± 0.1	1.4
			14.9	1.7 ± 0.2	1.0
2	22 54 19.04	61 45 47.3	1.5	3.4 ± 0.2	2″.2 × 0″.3 (42°)
			4.9	7.5 ± 0.1	1.1 × 0.3 (43°)
			14.9	15.8 ± 0.3	0.6 × 0.2 (41°)
3b	22 54 18.74	61 45 42.9	1.5	4.2 ± 0.1	1″.1
			4.9	5.0 ± 0.1	0.9
			14.9	4.1 ± 0.2	0.7
3c	22 54 19.02	61 45 43.9	1.5	2.1 ± 0.1	...
			4.9	3.7 ± 0.1	0.4
			14.9	5.2 ± 0.2	0.4
3d	22 54 19.26	61 45 43.9	1.5	4.7 ± 0.1	1.8 × 0.3 (102°)
			4.9	7.7 ± 0.1	1.3 × 0.2 (110°)
			14.9	8.9 ± 0.2	1.0 × 0.1 (108°)
4	22 54 19.56	61 45 53.9	1.5	4.2 ± 0.2	4.3 × 1.4 (82°)
			4.9	4.4 ± 0.1	4.8 × 1.2 (86°)
			14.9	2.5 ± 0.3	5.5 × 0.7 (75°)
5	22 54 20.77	61 45 57.4	1.5	2.0 ± 0.2	1″.9
			4.9	1.3 ± 0.1	...
			14.9	0.6 ± 0.2	...
6	22 54 21.25	61 46 0.8	1.5	4.3 ± 0.2	2.6
			4.9	3.8 ± 0.1	2.6
			14.9	2.3 ± 0.3	...
7a	22 54 21.22	61 45 37.7	1.5	9.5 ± 0.2	1.4
			4.9	9.6 ± 0.1	1.1
			14.9	6.9 ± 0.3	1.0
7b	22 54 21.81	61 45 37.4	1.5	4.5 ± 0.2	1.8
			4.9	2.8 ± 0.1	...
			14.9	1.9 ± 0.3	...
7c	22 54 22.42	61 45 35.2	1.5	4.5 ± 0.1	1.8
			4.9	3.8 ± 0.1	...
			14.9	1.8 ± 0.2	...
Variable Sources					
3a	22 54 18.14	61 45 41.8	1.5	~0.12	...
			4.9[c]	0.15	...
			4.9[d]	0.4 ± 0.1	0.7
			14.9	0.4 ± 0.1	0.7
8	22 54 18.75	61 45 44.9	1.5	~0.56	...
			4.9[c]	<0.12	...
			4.9[d]	0.64 ± 0.05	1.2
			14.9	<0.16	...
9	22 54 19.70	61 45 45.6	1.5	...	...
			4.9[c]	<0.16	...
			4.9[d]	3.0 ± 0.1	0.0
			14.9	2.9 ± 0.2	0.0

[a] Geometric mean of deconvolved major and minor axes, unless given explicitly. Values in parentheses indicate P.A. of direction of elongation.

[b] For nonvariable sources the flux density given at 4.9 GHz corresponds to the average of the values observed in July and December.

[c] 1991 July flux density.

[d] 1991 December flux density.

~0.04 pc. The easterly string (hereafter string 7) shows three peaks of emission (sources 7a, 7b, 7c) embedded in a line of diffuse emission, best appreciated in the 20 cm map. Source 7d of Hughes & Wouterloot (1984) is also detected, but it is very faint. The full length of string 7 is ~16″ (~0.06 pc at 725 pc). Sources 4, 5, and 6, which form the northern string, are characterized by irregular morphologies of weak and diffuse emission. Sources 4 and 6 show clumpy structure, which can be decomposed into two and three clumps, respectively. The knotty structure of these objects is similar to that observed in HH objects (Mundt 1988).

The radio sources at the center of the Cep A East region (objects 2, 3b, 3c, 3d) are, on the other hand, characterized by being brighter and more compact than the string sources. Objects 2 and 3d are elongated in one direction but unresolved in the orthogonal direction; object 3c is barely

resolved at 2 cm. It is worthy to note at this point that the deconvolved size of the major axes of sources 2 and 3d decreases with increasing frequency (see Table 2). We emphasize that our maps at the different frequencies were made with nearly the same UV coverage, so the difference in size scale at the different frequencies is real. A discussion of the dependence of angular size with frequency for these sources is presented in § 4.1. Of the variable sources, object 9 is unresolved while objects 3a and 8 are marginally resolved.

3.1.3. *Spectral Indices*

We used our 20 cm (L band), 6 cm (C band), and 2 cm (U band) maps, made with identical beams, to make spectral-index images with the AIPS task COMB. Here, the spectral index α is defined by $S_\nu \propto \nu^\alpha$, where S_ν is the flux density and ν is the frequency. In order to optimize the sensitivity to low surface brightness emission, the data were Gaussian-convolved to an angular resolution of 1".4. The spectral-index images reveal that the radio emission from the compact components within Cep A East span a wide range in spectral indices, from about -0.6 to ~ 1.0. See Figure 3 (Plate 2), which shows the α_{L-U} image. Toward sources 1a, 5, 7b, and 7c, spectral indices in the range -0.6 to 0.0 are seen, indicating a mixture of thermal and nonthermal emission. Sources 1b, 4, 6, and 7a have spectral indices in the range $-0.3 \leq \alpha \leq 0.1$, consistent, within the errors, with the value expected for optically thin free-free emission of -0.1. The spectral indices toward sources 2, 3b, 3c, and 3d are positive ($\alpha \geq 0.3$), with object 2 exhibiting the highest value.

The spectral indices of the integrated flux density from each nonvariable object, which includes the emission from both the brighter cores and from the diffuse envelopes, are given in Table 3. The integrated flux densities were computed by use of the task IMEAN, integrating over the area encompassed by the boxes shown in Figure 1. Columns (2), (3), and (4) give the spectral indices between pairs of frequencies while column (5) gives the overall spectral index obtained from a least-squares fit to the observed spectrum. This last ranges from -0.6 to 0.7. In Table 3 we also give the spectral indices at the position of the peak emission (cols. [6]–[8]). The observed integrated flux density versus frequency of the nonvariable radio sources within the Cep A East region and the result of the fits are shown in Figure 4. We note that the spectral indices of the emission from the diffuse envelopes of the string sources are slightly different (usually more negative) than those of the emission from their more compact cores. A discussion of the spectral indices is presented in § 4.1.

A comparison with previous determinations of spectral indices of the integrated emission between 20 and 6 cm shows that there is good agreement between the values reported for the most compact sources but significant differences between the values given for the more diffuse objects. For example, for the compact sources 2 and 3d, Hughes (1985) reported α_{L-C} indices 0.64 and 0.35, respectively, similar to the values derived in this work of 0.68 and 0.42. The largest differences are found for sources 1a + 1b, 5, and 7b, for which Hughes (1985) reported α_{L-C} indices of -0.14, 0.37, and 0.07, respectively, while we derived values of -0.31, -0.41, and -0.42. However, for these same objects, using the values of the flux densities reported by Hughes & Wouterloot (1984; see their Table 1) we find α_{L-C} indices of -0.37, -0.01, and -0.34 for sources 1a + 1b, 5, and 7b, respectively, in better agreement with the values reported in this work. Further, if we use the values of the flux densities reported by Hughes (1985), sources 1b and 7a appear to have spectral indices of -1.0 and -0.3, respectively. In retrospect, it seems that there was some evidence for the presence of negative spectral indices among the radio emission from the string sources, but this was not mentioned or discussed in the previous works.

3.2. *Cep A West*

In Figure 5 we show the matching-beam maps of the radio emission, at wavelengths of 20 and 6 cm, from the Cep A West region. The primary half-power beamwidth of the 2 cm observations does not include this region, and thus only 20 and 6 cm observations are discussed. Its radio morphology consists of two compact components (W-1 and W-2) located toward the southeast and an extended, diffuse component (W-3) located toward the northwest. The components are designated with the same numbers as given by Hughes (1989). The extended component exhibits a weak, diffuse envelope, clearly seen in the 20 cm map, and a relatively brighter core, best appreciated in the 6 cm image. We note that, since the Cep A West region is located $\sim 60''$ from the phase center of our observations, the maps of Cep A West are affected by bandwidth smearing. At 20 cm and 6 cm the Cep A West sources are broadened angularly by

TABLE 3

SPECTRAL INDICES

	INTEGRATED EMISSION				PEAK EMISSION		
SOURCE (1)	α_{L-C} (2)	α_{L-U} (3)	α_{C-U} (4)	α_{LCU}[a] (5)	α_{L-C} (6)	α_{L-U} (7)	α_{C-U} (8)
1a	−0.55	−0.59	−0.62	−0.59	−0.23	−0.38	−0.53
1b	−0.09	−0.27	−0.45	−0.27	−0.01	−0.20	−0.40
2	0.68	0.67	0.66	0.67	0.96	0.89	0.82
3b	0.15	−0.01	−0.18	−0.01	0.20	0.06	−0.09
3c	0.46	0.39	0.32	0.39	0.55	0.46	0.37
3d	0.42	0.28	0.13	0.28	0.63	0.44	0.23
4	0.06	−0.22	−0.51	−0.22	0.04	−0.15	−0.36
5	−0.41	−0.51	−0.62	−0.51	−0.02	...	...
6	−0.09	−0.28	−0.48	−0.28	0.02	−0.23	−0.48
7a	0.02	−0.14	−0.30	−0.14	0.20	−0.01	−0.24
7b	−0.42	−0.37	−0.32	−0.37	−0.37	−0.31	−0.24
7c	−0.14	−0.39	−0.65	−0.39	0.26	−0.09	−0.46

[a] From a least-squares fit to the spectrum.

PLATE 2

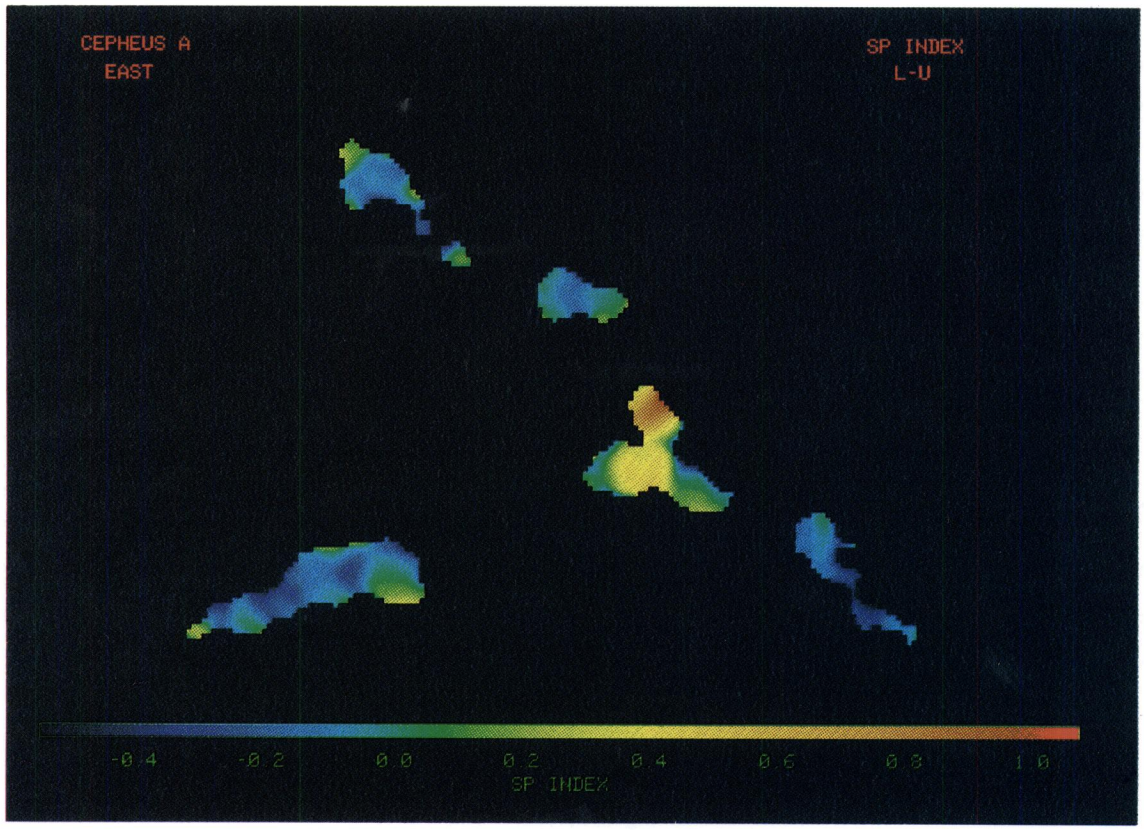

FIG. 3.—Image of the α_{L-U} spectral index of the radio emission from the Cep A East compact radio sources. The image is centered at $\alpha = 22^h54^m19^s.84$, $\delta = 61°45'47''.1$ and covers an angular extent of $61'' \times 46''$. A bar indicating the spectral-index color scale, which ranges from -0.6 to 1.0, is shown at the bottom.

GARAY et al. (see 459, 197)

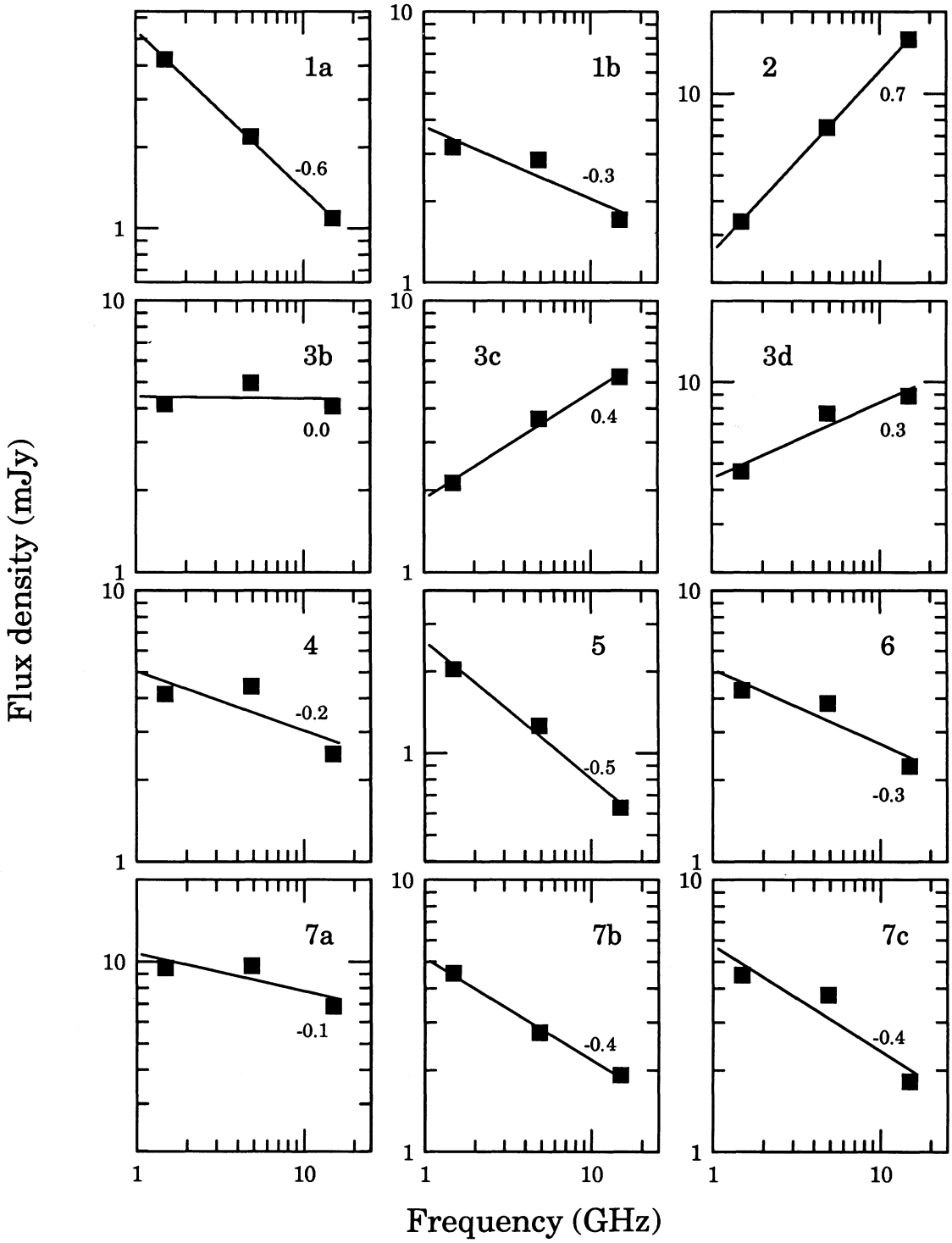

FIG. 4.—Radio continuum flux density vs. frequency for the nonvariable radio sources within the Cep A East region. In each panel the line represents a minimum least-squares power-law fit to the observed spectra of the object indicated at the top. Also given is the fitted power-law index.

$\sim 1''.8$ and $\sim 1''.1$, respectively, in the radial (with respect to the phase center) direction. Bandwidth smearing, however, does not affect the integrated flux densities. In Table 4 we list the positions, flux densities, deconvolved sizes, and spectral indices in the 1.5–4.9 GHz range of the Cep A West sources.

The spectra of the integrated and peak emission from the three objects are presented in Figure 6. The spectral indices of the peak and integrated emission are significantly different for sources W-2 and W-3. For source W-2, the spectral index of the integrated emission is 0.1 ± 0.1 while that of the peak emission is 0.6 ± 0.1, which suggests the presence of an ultracompact, probably optically thick, source at its center. We note that, since bandwidth smearing produces a decrease in the peak flux density and is more important at 20 cm, the value of the α_{L-C} index for the peak flux density, 0.6, is probably an upper limit. For the extended W-3 component, the spectral index of the integrated emission is

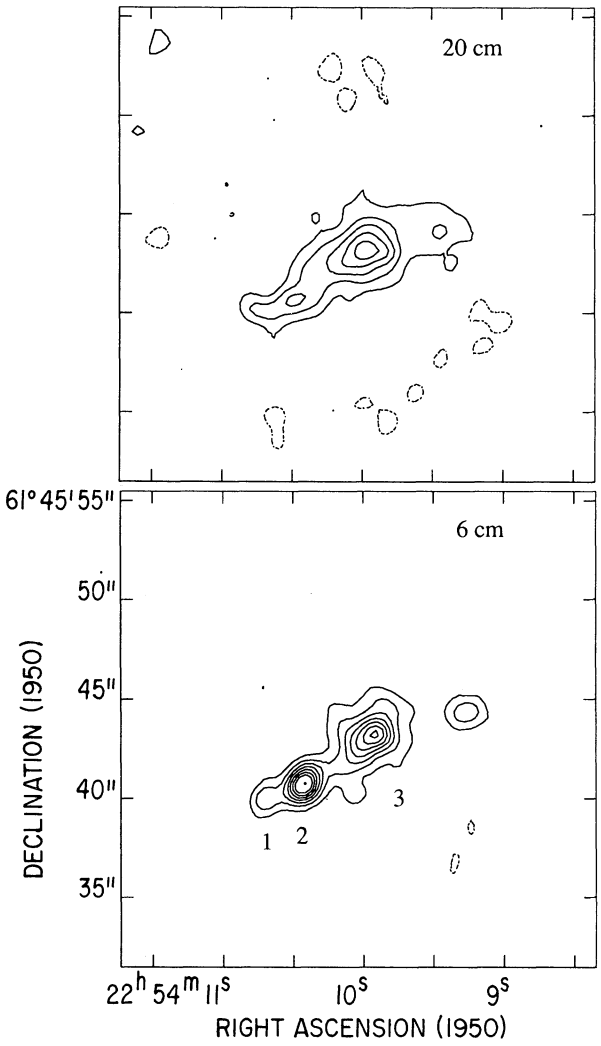

FIG. 5.—VLA radio continuum maps of the Cep A West region with 1.″2 angular resolution. *Top*: 20 cm map. Contour levels are −1, 1, 2, 3, 4, and 5 × 0.15 mJy beam^{-1}. *Bottom*: 6 cm map. Contour levels are −1, 1, 2, 3, 5, and 7 × 0.1 mJy beam^{-1}.

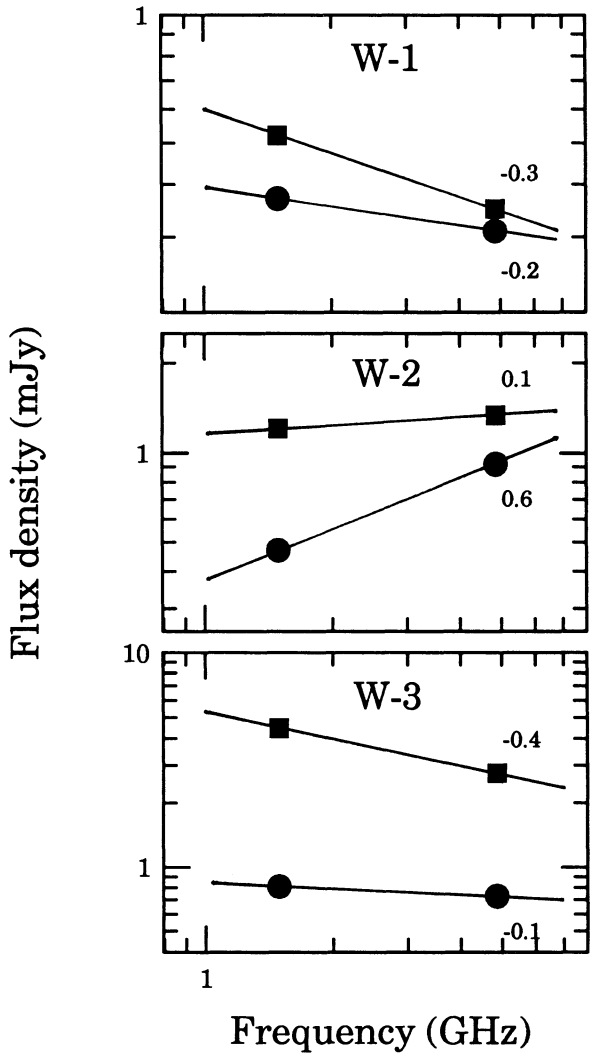

FIG. 6.—Radio continuum flux density vs. frequency for the Cep A West radio sources. Circles and squares represent the observed peak and integrated emission, respectively.

-0.4 ± 0.1 while that of the peak emission is -0.1 ± 0.1, which suggests that a synchrotron emission component may coexist with free-free emission.

We also detected radio emission from the brightest Hα knot within GGD 37, object S of Hartigan & Lada (1985), located ~1′ northwest of object W-3. The parameters measured by us for this source are given in Table 4. Radio emission and proper motion of object S were previously reported by Hughes & Moriarty-Schieven (1990).

3.3. *Other Radio Sources*

Beyond the 25″ radius region that contains the Cep A East compact objects, we detected three compact radio sources. Their positions, flux densities, and sizes are given in

TABLE 4

OBSERVED PARAMETERS OF CEPHEUS A WEST SOURCES

SOURCE	POSITION (1950) α	POSITION (1950) δ	FREQUENCY (GHz)	FLUX DENSITY (mJy)	ANGULAR SIZE[a]	α_{L-C}
W1	22h54m10.s70	61°4′40.″0	1.5	0.5 ± 0.1	0.″0 × 0.″0	−0.33
			4.9	0.4 ± 0.1	...	
W2	22 54 10.43	61 45 40.8	1.5	1.2 ± 0.1	...	0.09
			4.9	1.3 ± 0.1	0.″9	
W3	22 54 9.96	61 45 43.1	1.5	4.5 ± 0.2	3.″7 × 2.″4 (119°)	−0.40
			4.9	2.8 ± 0.1	3.0 × 1.8 (133°)	
S	22 54 3.00	61 45 58.9	1.5	1.0 ± 0.2	...	0.04
			4.9	1.0 ± 0.1	2.″4	

[a] Geometric mean of deconvolved major and minor axes, unless given explicitly. Values in parentheses indicate P.A. of direction of elongation.

TABLE 5

OBSERVED PARAMETERS OF FIELD SOURCES

SOURCE	POSITION (1950) α	POSITION (1950) δ	FREQUENCY (GHz)	FLUX DENSITY (mJy)	ANGULAR SIZE
C1.....	$22^h54^m15^s.07$	61°46′15″.8	1.5	0.13	0″.0 × 0″.0
			4.9	0.43	0.0 × 0.0
C3.....	22 54 14.92	61 45 39.5	1.5	0.38	...
			4.9	0.29	1.0 × 0.4
C4.....	22 54 28.03	61 46 18.6	1.5	1.18	2.2 × 0.6 (75°)[a]
			4.9	0.50	0.0 × 0.0

[a] Value in parentheses is P.A. of direction of elongation.

Table 5. Two of them (sources C1 and C3) were previously reported by Hughes & Moriarty-Schieven (1990). The flux density of the third, newly reported, source (labeled C4) has a spectral index between 1.5 and 4.9 GHz of −0.7, which suggests it may correspond to a background extragalactic object.

4. DISCUSSION

4.1. *The Nature of the Radio Sources within the Cep A East Region*

There is an unusually high density of compact radio sources within the Cep A East region: Hughes and collaborators have identified 16 compact radio sources in a region ~25″ in radius, centered near the H_2O maser activity (Lada et al. 1981). Based on many different lines of evidence, we argue below that there are two types of radio sources within this region: internally excited and externally excited objects. In what follows we discuss the characteristics of the sources in these two groups separately.

4.1.1. *Objects that Harbor an Energy Source*

The radio sources within this group are objects 2, 3a, 3c, 3d, 8, and 9. Indications of the presence of an internal source of energy within each of these objects include their association to H_2O and OH maser condensations (objects 2, 3a, 3d; Lada et al. 1981; Cohen et al. 1984), large variability in their flux densities (objects 3a, 8, 9; Hughes 1988, 1991; this paper), positive spectral indices (objects 2, 3c, 3d; this paper), and association to IR point sources (object 3a; Lenzen 1988). Even though these sources share similar characteristics in the radio band, such as being the most compact and brighter within the Cep A East region, they appear to have different physical characteristics.

4.1.1.1. Source 2

This elongated radio object is believed to be associated with the most luminous (~10^4 $L_\odot$) source in the region. A detailed discussion of its observed characteristics in the frequency range from 1.5 to 43 GHz and physical nature has been presented elsewhere (Rodríguez et al. 1994). In summary, we found that the flux density of source 2 increases with frequency as $\nu^{0.7}$, while the angular size of its major axis decreases with frequency as $\nu^{-0.6}$. The above frequency dependences are very close to the theoretical values of $\nu^{0.6}$ and $\nu^{-0.7}$ expected for a biconical thermal jet and make source 2 the best example known of this type of object. Recent observations made with high angular resolution (Hughes, Cohen, & Garrington 1995; Hoare & Garrington 1995) show that the morphology of source 2 is clumpy, consisting of at least four components that form a structure elongated in a direction with a position angle of 45° ± 3°, in good agreement with the value derived by Rodríguez et al. (1994). To explain the clumpy morphology, Hughes et al. (1995) suggested that the mass loss from the central object is not continuous but occurs in episodic events.

An additional result, presented here, is that the spectral index of the emission from source 2 is not constant along its major axis, but decreases toward the edges. The change in spectral index is illustrated in Figure 7, which shows cuts of the L, C, and U maps and of the L−C and L−U spectral-index images along the semimajor axis. The spectral indices reach maximum values ($\alpha_{L-C} = 0.96 \pm 0.03$, $\alpha_{L-U} = 0.89 \pm 0.02$) at the position of the ultracompact sources detected by Hughes (1988) (indicated by an arrow in the lower left panel) and decrease toward the edges of the elongated structure, reaching values of ~0.1. This result is consistent with the fact that the jet is resolved, in which case the spectral-index images should show regions of totally opaque ($\alpha = 2$) emission at their centers, totally transparent ($\alpha = -0.1$) emission at their borders, and intermediate indices at spatially intermediate regions (Reynolds 1986). It is the spatially integrated emission from these different regions that gives rise to the 0.6 spectral index. In Figure 7 we also show the "one-dimensional flux density"—intensity integrated along a direction perpendicular to the major axis—at the frequencies of 1.5, 4.9, and 15 GHz and the corresponding spectral indices, as a function of distance along the major axis, for a jet model (see Rodríguez et al. 1990) with $\epsilon = 1.2$, $\tau_o = 0.12$, and $I_o = 5.2$ mJy arcsec^{-1}. The parameter ϵ corresponds to the power-law index that describes the dependence of the jet half-width (perpendicular to the jet axis) with the distance to the jet's origin while τ_o is the optical depth at 1 GHz and at 1″ from the jet center for a line of sight perpendicular to the major axis. Since we are observing the jet with a beam of 1″.2, we also show the resulting convolved model. This model gives flux densities and spectral indices that are in excellent agreement with the observations.

4.1.1.2. Source 3a

This source coincides with a weak 1 μm point source detected by Lenzen (1988) and is associated with an H_2O maser spot (Cohen et al. 1984). At 5 GHz we barely detected source 3a during 1991 July ($S_{5\,GHz} \sim 0.15$ mJy); in 1991 December we measured a flux density of 0.42 mJy. Comparison with the observations of Hughes (1988) shows that object 3a undergoes significant variations in its flux density. These characteristics suggest that source 3a might be a low-

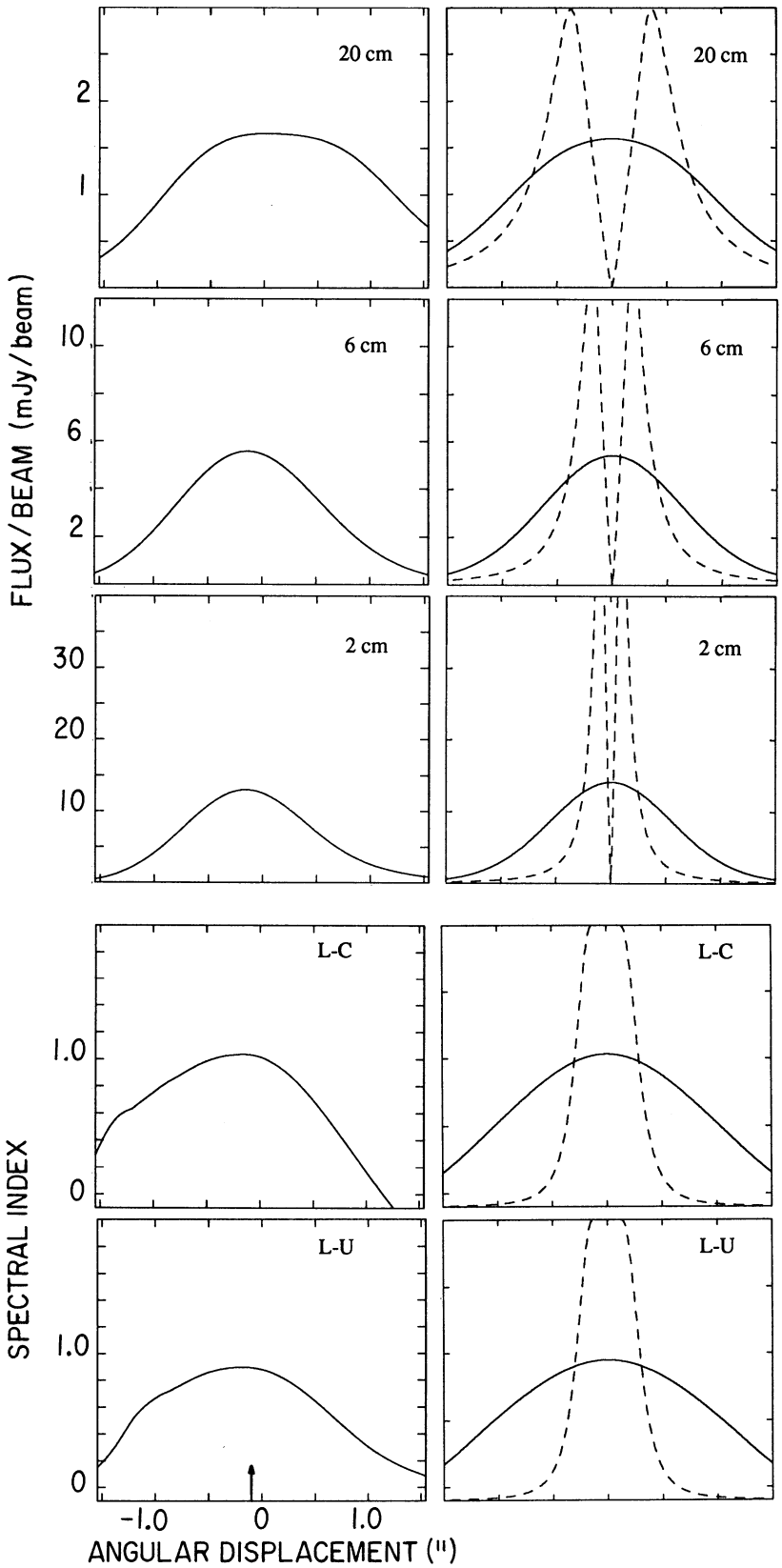

FIG. 7.—*Left*: One-dimensional slices of the flux density per beam and spectral-index maps along the major axis of source 2. From top to bottom, slice of the 20 cm map, 6 cm map, 2 cm map, L − C spectral-index map, and L − U spectral-index map. The arrow in the bottom panel indicates the position of the ultracompact sources detected by Hughes (1988). *Right*: Same as above, but for the bipolar-jet model discussed in § 4.1.1.1. The dashed lines represent the results of the model with 0.″05 angular resolution; the solid lines correspond to the model results convolved with 1.″2 angular resolution (for comparison with the left panels).

luminosity young star with nonthermal emission located within the central region of star formation.

4.1.1.3. Source 3c

Our observations at 15 GHz show that source 3c is barely resolved (deconvolved FWHM angular diameters of $0''.57 \times 0''.24$) and has a flux density of 5.0 mJy. Observations at the same frequency with angular resolution of $0''.1$, made by Hughes (1988), show that it has an unresolved, ultracompact core (FWHM angular diameter less than $0''.1$) with a flux density of 2.7 mJy. We find that the total flux density of source 3c, in the 1.5–15 GHz range, is well fitted by a power law of the form $S_\nu \propto \nu^{0.4 \pm 0.1}$. The positive value of the spectral index, as well as the presence of an ultracompact component, suggest that this source is internally excited and, hence, that it is associated with a star.

4.1.1.4. Source 3d

Our maps show that this object is elongated in a direction at a P.A. of $107° \pm 4°$ and unresolved in the orthogonal direction (see Table 2). We find that the deconvolved FWHM major axis decreases with increasing frequency (see Table 2) as $\theta_\nu \propto \nu^{-0.28 \pm 0.05}$. The deconvolved size at 15 GHz, $0''.97 \times 0''.11$, indicates an elongation ratio of ~ 9 and an opening angle (for a jetlike geometry) equal to or smaller than 13°. A power-law fit to the flux density versus frequency dependence in the 1.5–15 GHz range gives $S_\nu \propto \nu^{0.28 \pm 0.08}$. We note, however, that a single–power-law fit to the radio continuum spectra is inadequate (see Fig. 4). The spectral index in the lower frequency range ($\alpha_{L-C} = 0.42 \pm 0.03$) is significantly larger than that in the high-frequency range ($\alpha_{C-U} = 0.13 \pm 0.03$).

Observations at 15 GHz with an angular resolution of $0''.1$ (Hughes 1988) show that the core of this source consists of two unresolved, ultracompact components (FWHM angular diameters less than $0''.1$) separated by $\sim 0''.2$. The line joining the two ultracompact sources is at a P.A. of $114° \pm 5°$, roughly in the same direction as that of the elongation of the extended structure seen in our maps. The total flux density at 15 GHz measured by Hughes (1988), 3.5 mJy, is $\sim 45\%$ of the total flux density observed by us with 10-fold lower angular resolution, which shows that the emission from the extended structure seen in our observations is resolved out at resolutions of $0''.1$.

The above results are suggestive of a thermal-jet nature for object 3d. The power-law dependences with frequency of the angular size and flux density are similar to those derived for the exciting source of the HH 80–81 system of Herbig-Haro objects (Martí, Rodríguez, & Reipurth 1993). The observed dependences cannot, however, be explained by a simple jet model with constant temperature, velocity, and ionization fraction. They may possibly be explained by assuming that one or more of these parameters varies with the distance from the jet center (Reynolds 1986). Finally, we mention that, as for object 2, the spectral index of the radio emission along the major axis of object 3d is not constant but decreases toward the edges.

4.1.1.5. Sources 8 and 9

The radio emission from both these sources is highly variable. Hughes (1988) observed object 8 at 5 GHz in three epochs, over a period of 5 yr, and found that its flux density varied from 0.28 mJy in 1981 to less than 0.1 mJy in 1982 and to 0.47 mJy on 1986. In 1991 December we measured a flux density of 0.64 mJy at 5 GHz and an upper limit of 0.27 mJy at 15 GHz. Source 9 was observed by Hughes (1991) in four epochs, over the period 1988 November–1990 May, and found that the 5 GHz flux density varied from epoch to epoch, being in the range 0.3–2.4 mJy. The 5–15 GHz spectral index also varied, being in the range between -0.6 and 0.2, which suggests a nonthermal nature for the radio emission. During 1991 December, we measured a flux density at 5 GHz of 3.0 mJy and a spectral index between 5 and 15 GHz of 0.0 ± 0.1. Hughes (1988, 1991) has discussed possible interpretations of the radio emission from these objects, and we will not discuss them further. In short, the radio-emission mechanism has not yet been conclusively established but is likely to be gyrosynchrotron emission originating close to the stellar surface.

Surveys of star-forming regions at radio wavelengths show that the kind of flare activity exhibited by sources 8 and 9 is characteristic of low-mass, pre–main-sequence stars (André, Montmerle, & Feigelson 1987; Garay, Moran, & Reid 1987; Montmerle & André 1988), which suggests that these two sources may be associated with recently formed low-mass stars. In addition, radio surveys of pre–main-sequence stars known to be associated with phenomena of mass ejection (jets, winds, HH objects) show that they are usually detected and that their radio emission has the characteristics of free-free emission. Even though the radio emission from sources 8 and 9 seems to have a nonthermal origin, they cannot be ruled out as potential candidates for being driving sources of some of the activity seen toward the Cep A East region (Hughes et al. 1995).

4.1.2. *Objects Excited by an External Source of Energy*

4.1.2.1. String Sources

The radio sources within this group (objects 1a, 1b, 4, 5, 6, 7a, 7b, 7c, 7d) are characterized by being less bright than the internally excited sources, by exhibiting extended halos of diffuse emission, and by being found in chains or strings. A notable characteristic of these sources is that they are located at the edges of dense ammonia condensations (Torrelles et al. 1993). String 1 is projected toward the northern edge of the NH_3 clump Cep A-1, string 7 is projected toward the southern border of Cep A-3, and the northern string is at the southern edge of the NH_3 clump Cep A-2.

The spectral indices of the integrated emission from sources 1b, 4, 6, and 7a are between -0.3 and -0.1. They are somewhat smaller, but consistent within the errors, with those expected for optically thin thermal emission. In Table 6 we list the derived parameters (electron density, emission measure EM, optical depth, and number of ionizing photons N_i) for these sources, assuming that their emission is thermal radiation from a plasma with an electron temperature of 10^4 K. On the other hand, the spectral indices of the integrated radio emission from string sources 1a, 5, 7b, and 7c, ≤ -0.4, are characteristic of nonthermal emission. Rodríguez et al. (1993) have shown that sharply negative spectral indices cannot occur for free-free emission, regardless of the electron density and temperature distribution. Radio sources with large negative spectral indices within star-forming regions have already been found by Rodríguez et al. (1989), Yusef-Zadeh et al. (1990), Martí et al. (1993), Curiel et al. (1993), and Reid et al. (1995).

TABLE 6

PARAMETERS OF STRING SOURCES

A. Thermal Sources

	OBSERVED			DERIVED			
SOURCE	ν (GHz)	S_ν (mJy)	θ_s	n_e (10^4 cm^{-3})	EM (10^6 pc cm^{-6})	τ	N_i (10^{44} s^{-1})
1b.....	4.9	2.9	1".4	1.0	0.7	0.008	1.3
4[a]	4.9	3.8	1.8	0.8	0.5	0.006	1.8
6[a]	4.9	1.8	0.8	1.7	1.2	0.015	0.85
7a.....	4.9	9.6	1.1	2.5	3.4	0.04	4.5

B. Nonthermal Sources

	OBSERVED			DERIVED		
SOURCE	ν (GHz)	S_ν (mJy)	θ_{sph}	B (mG)	$n_{er} E_{min}$ (10^{-9} ergs cm^{-3})	n_{er} (10^{-4} cm^{-3})
1a.....	1.5	4.2	4".1	0.30	0.72	4.5
5	1.5	2.0	3.8	0.26	0.54	3.4
7b.....	1.5	4.5	3.6	0.34	0.94	5.8
7c.....	1.5	4.5	3.6	0.34	0.93	5.8

[a] Observed and derived parameters for the brightest clump within the source.

Most of the string sources show a mixture of positive, flat, and negative spectral indices across their faces, which suggests that both thermal and nonthermal emission arises from the strings. This combined thermal and nonthermal emission can be expected from a shock wave moving through a magnetized medium, where a fraction of the electrons will be accelerated to relativistic velocities, producing the nonthermal synchrotron emission, while most of the electrons (with a thermal distribution of velocities) will produce the thermal free-free component (Crusius-Wätzel 1990; Henricksen, Ptuskin, & Mirabel 1991). A similar scenario has been proposed by Curiel et al. (1993) to explain a similar mixture of positive, flat, and negative spectral indices observed in the Serpens radio jet. In both cases, the flat and positive spectral indices are associated with the brighter knots while the negative indices appear to be associated with the faint and extended emission between the clumps, and there seems to be a gradual transition between positive and negative indices (at least at the observed angular resolution). On the other hand, there are notable differences between Cep A and the Serpens radio jet. The Cep A complex is being powered by a young, high-luminosity star(s) ($L_b \sim 2 \times 10^4\ L_\odot$) while the energy source of the Serpens radio jet is a young, low-luminosity star with probably a similar mass-loss rate but slower wind velocity (of about a few hundred km s^{-1}). Some of the knots of the Serpens radio jet have proper motions of $\sim 0''.12$ yr^{-1} (~ 200 km s^{-1} at a distance of ~ 300 pc; Rodríguez et al. 1989; Curiel et al. 1993). In the Cep A region, we have not observed proper motions in any of the knots. Comparing the present observations with previous observations obtained in the past 10 yr by Hughes and collaborators and by us, we obtain an upper limit for the proper motions of the knots of $\sim 0''.02$ yr^{-1} (or velocities smaller than 70 km s^{-1} at the adopted distance of 725 pc). These results suggest that although the origin of the radio thermal and nonthermal emission in both regions is the same (the radio emission is produced by electrons accelerated and compressed in a shock wave), the origin of the emitting shock wave seems to be different. The knotty structure of the Serpens radio jet has been interpreted as the result of discrete ejection of material (time-variable wind or "bullets") from the central source, where the radio emission is produced by the shock wave preceding the condensations moving through the ambient medium. In the Cep A case, the lack of proper motions suggests that the radio emission is either produced by condensations moving at steep angles with respect to the plane of the sky (almost along the line of sight) or that the shock waves are quasi-static with respect to the ambient medium.

1. *Nonthermal emission.*—Henriksen et al. (1991) have shown that the radio emission that arises from the region of interaction between an outflow and the ambient cloud material would be either thermal or nonthermal, depending on the density and temperature of the lobes. If the thermal density is below the thermal critical density n_e^{th}(crit), given by

$$\left[\frac{n_e^{th}(\mathrm{crit})}{\mathrm{cm}^{-3}}\right] = 2.1 \times 10^4 \left[\frac{\alpha(p)}{g_{ff}}\right]^{1/2} \left(\frac{T_e}{10^4\ \mathrm{K}}\right)^{1/4} \left(\frac{B}{\mathrm{mG}}\right)^{3/4} \times \left(\frac{E_{min}}{10^{-6}\ \mathrm{ergs}}\right)^{1/2} \left(\frac{\nu}{\mathrm{GHz}}\right)^{-1/4} \times \left(\frac{n_{er}}{10^{-3}\ \mathrm{cm}^{-3}}\right)^{1/2}, \quad (1)$$

where n_{er} is the density of the nonthermal electrons, B is the magnetic field, T_e is the electron temperature, and E_{min} is the minimum energy of the relativistic electrons, then the synchrotron radiation will dominate the free-free radiation. The quantity g_{ff} is the Gaunt factor for free-free emission, and $\alpha(p)$, where p is the energy spectral index, is the standard synchrotron radiation factor as defined by Lang (1980). The production of relativistic electrons is understood in terms of a diffusive shock-wave acceleration mechanism, in which the electrons are accelerated by traversing the shock many times because of scattering off magnetohydrodynamic irregularities (see Crusius-Wätzel 1990). The theory of this mechanism has been reviewed by Bland-

ford & Eichler (1987). For a strong shock, a synchrotron spectral index close to -0.5 is expected.

We propose that the radio emission from the diffuse envelopes of the string sources corresponds to synchrotron radiation from electrons that are accelerated in the region of interaction between the wind from a central star and the ambient cloud material. The density of relativistic particles and the magnetic field needed to account for the observed nonthermal radiation can be estimated as follows. The theory of diffusive shock-wave acceleration shows that in the steady state case the energy distribution of the relativistic electrons is a power law, $n(E) \propto E^{-p}$, where the index p depends on the shock characteristics (see Blandford & Eichler 1987; Crusius-Wätzel 1990), producing a synchrotron spectrum $S_\nu \propto \nu^{-(p-1)/2}$. Assuming that $p = 2$ (which implies a spectral index of -0.5, similar to the observed values) and that there is equipartition of energy between the magnetic field and the particle energy, then for a synchrotron source with an angular diameter $\theta_{\rm sph}$ and a flux density S_ν, the magnetic field strength and the product of the density times the minimum energy of the relativistic electrons are given by

$$\left(\frac{B}{\rm mG}\right) = 0.50\left(\frac{S_\nu}{\rm mJy}\right)^{2/7}\left(\frac{\theta_{\rm sph}}{\rm arcsec}\right)^{-6/7}\left(\frac{\nu}{10\ {\rm GHz}}\right)^{1/7} \times \left(\frac{D}{\rm kpc}\right)^{-2/7}\left(\log\frac{E_{\rm max}}{E_{\rm min}}\right)^{2/7}, \quad (2)$$

$$\left(\frac{n_{\rm er}\,E_{\rm min}}{10^{-9}\ {\rm ergs\ cm^{-3}}}\right) = 3.58\left(\frac{S_\nu}{\rm mJy}\right)\left(\frac{\theta_{\rm sph}}{\rm arcsec}\right)^{-3}\left(\frac{\nu}{10\ {\rm GHz}}\right)^{1/2} \times \left(\frac{D}{\rm kpc}\right)^{-1}\left(\frac{B}{\rm mG}\right)^{-3/2}, \quad (3)$$

where D is the distance to the source and $E_{\rm max}$ is the maximum energy of the relativistic electrons. In Table 6 we list the magnetic field and density of relativistic electrons derived for the string sources with the largest negative spectral indices, computed from the above expressions and adopting minimum and maximum energies of 10^6 and 10^{11} eV, respectively, and a distance of 0.725 kpc. For angular diameter we used the geometric mean of the major and minor angular diameters observed at 1.5 GHz, since at this frequency better estimates of the sizes can be made.

The strength of the magnetic field within the string sources is typically ~ 0.3 mG and the density of relativistic electrons $\sim 5 \times 10^{-4}$ cm^{-3}. From the identification of the Zeeman pattern in OH lines, Wouterloot, Habing, & Herman (1980) derived a magnetic field of 3.5 mG for the OH maser clumps within Cep A East. Evidence for a decay of the magnetic field in the OH maser region, probably due to expansion of gas around a young star, has been presented by Cohen, Brebner, & Potter (1990). It is interesting to note that the magnetic field strength scales with density, from the conditions found at the edge of the NH_3 molecular clouds ($B \sim 0.3$ mG, $n \sim 2 \times 10^4$ cm^{-3}) to those found in the OH masers—thought to have molecular densities of $\sim 10^7$ cm^{-3} (see Reid & Moran 1981)—roughly as $B \propto n^{0.4}$. This result suggests that the magnetic field has its origin in the general interstellar field and tends to support current theories of magnetic field compression during protostellar contraction that predict that $B \propto n^{0.5}$ (see Mouschovias 1976).

The detection of nonthermal and thermal emission from different regions of a string feature allows one to draw interesting implications on the critical thermal density. To illustrate this point, we consider the observations of sources 7a and 7b, the former exhibiting a flat spectrum, suggestive of thermal emission, the latter having a large negative spectral index, suggestive of nonthermal emission. Assuming that the emission from source 7b is entirely nonthermal, we derived (see Table 6) $B = 0.34$ mG and $n_{\rm er}E_{\rm min} = 9.4 \times 10^{-10}$ ergs cm^{-3}. Replacing these values in equation (1), using $\alpha(2) = 2.06$ and $g_{\rm ff} = 5.76$, we find that the critical density is 5.0×10^3 cm^{-3}. The expectation then is that the density of the thermal electrons within source 7a should be higher than this critical density, which is in agreement with the derived value of 2.5×10^4 cm^{-3} (see Table 6).

2. *Thermal emission from shocks.*—Curiel, Cantó, & Rodríguez (1987) calculated the expected thermal radio continuum emission produced in a shock wave as seen from an observer that is either on the side of the recombination zone or on the side of the cooling zone. In the optically thin regime, the flux density is given by (see also Curiel et al. 1989, 1993)

$$\left(\frac{S_\nu}{\rm mJy}\right) = 0.98\left(\frac{\nu}{10\ {\rm GHz}}\right)^{-0.1}\left(\frac{\theta_s}{\rm arcsec}\right)^{2}\left(\frac{T_e}{10^4\ {\rm K}}\right)^{0.45} \times \left(\frac{n_o}{10^3\ {\rm cm^{-3}}}\right)\left(\frac{v_o}{10^3\ {\rm km\ s^{-1}}}\right)^{1.68}, \quad (4)$$

where n_o is the preshock density, v_o is the shock velocity and θ_s is the source's angular diameter. Most of the radio emission arises from the recombination zone, where the ionization is provided by photons produced in the cooling zone.

In the case that the shock wave is produced by a stellar wind impinging over an obstacle, n_o is the density of the stellar wind at the position of the obstacle, which for a jet wind with a half-width power index $\epsilon = 1$ is given by

$$\left[\frac{n_o(r)}{10^3\ {\rm cm^{-3}}}\right] = 0.42\left(\frac{\dot{M}_w}{10^{-6}\ M_\odot\ {\rm yr^{-1}}}\right)\left(\frac{v_w}{10^3\ {\rm km\ s^{-1}}}\right)^{-1} \times \left(\frac{\Theta_o}{\rm rad}\right)^{-2}\left(\frac{r}{0.01\ {\rm pc}}\right)^{-2}, \quad (5)$$

where r is the distance from the obstacle to the star, v_w is the velocity of the wind, $\dot{M}_w$ is the wind mass-loss rate, and Θ_o is the opening angle of the jet.

If one assumes that the radio emission from the string sources with flat spectrum is free-free emission from a shocked wind, then from the observed parameters and equations (4) and (5) it is possible to derive a condition between the mass-loss rate and the velocity of the required stellar wind. Using the observed parameters of source 1b ($S_\nu = 3.18$ mJy at 1.5 GHz, $\theta_s = 1''.6$), which is at an angular distance of $\sim 12''$ (or $r \sim 0.042$ pc) from source 2—the origin of the collimated thermal jet—we find $\dot{M}_{w,-6}\,v_{w,3}^{0.68} = 3.2$, where $\dot{M}_{w,-6}$ is the mass-loss rate in units of $10^{-6}\ M_\odot$ yr^{-1} and $v_{w,3}$ is the velocity in units of 10^3 km s^{-1}. On the other hand, modeling the observed radio emission from object 2 as arising from a biconical thermal jet of constant temperature, velocity, and ionization fraction, with a jet axis perpendicular to the line of sight, Rodríguez et al. (1994) found that the ionized mass-loss rate and velocity are related by the expression $\dot{M}_{w,-6}\,v_{w,3}^{-1} = 1.1$. Combining these two conditions implies that the jet stellar wind from source 2 has a mass-loss rate of $2 \times 10^{-6}\ M_\odot$ yr^{-1} and a velocity of 1900 km s^{-1}. The rate of injection of momentum

by the jet into the surrounding medium is then $\sim 4 \times 10^{-3}$ $M_\odot$ yr^{-1} km s^{-1}.

4.1.2.2. Source 3b

Source 3b has FWHM diameters of $\sim 1''.4 \times 0''.5$ and is elongated in a direction with a P.A. of $\sim 49°$. Its spectral index between 1.5 and 15 GHz is flat, indicative of optically thin thermal emission. From these characteristics it is difficult to discern whether object 3b is internally or externally ionized. If internally photoionized, the rate of ionizing photons required to explain the observed flux density, 2×10^{44} s^{-1}, implies the presence of an embedded B2 zero-age main-sequence star. Its elongation and location in a linear arrangement suggest, however, that the radio emission from object 3b may arise from shock-heated gas excited by the wind of a nearby source.

4.2. *The Nature of the Radio Sources within the Cep A West Region*

The overall morphology of the Cep A West radio source, which exhibits an extended region of diffuse emission (source W-3) flaring away from two compact components (sources W-1 and W-2), is reminiscent of that of a jet or collimated outflow. Further, the line joining sources W-1, W-2, and W-3 points toward the GGD 37 group of HH objects, located $\sim 50''$ northwest of the radio sources, providing additional support for the outflow hypothesis. In the following we discuss the nature of the radio sources within the Cep A West region.

4.2.1. *Source W-2*

Our observations show that the 1.5–5 GHz spectral index of the integrated radio emission from this source is 0.09 ± 0.11. The spectral index of the peak emission is, however, considerably larger, 0.57 ± 0.12, suggesting the presence of an ultracompact, optically thick component at its center. Hughes (1989) showed that source W-2 exhibits significant variations in its flux density. The above characteristics suggest that this source has an energy source of its own, which leads us to propose that object W-2 is the source of energy powering the activity seen in the direction of Cep A West (see discussion in § 4.3). This radio source has not been detected at optical or IR wavelengths, suggesting it may be associated with a low-luminosity pre–main-sequence star embedded within the molecular cloud.

4.2.2. *Source W-3*

The radio morphology of this source consists of a relatively bright central core surrounded by a diffuse halo of emission with angular diameters (FWHM) of $3''.7 \times 2''.4$. The envelope is elongated in a direction with a P.A. of 119° (see Table 4), roughly the same as that of the line joining the radio objects W-2, W-3, and the GGD 37 group of HH objects. At 1.5 GHz we measured a total flux density, including that of the diffuse emission toward the west, of 6.1 mJy. This value is $\sim 40\%$ smaller than the average flux density reported by Hughes (1989) from observations in three different epochs. The latter value has, however, a large dispersion ($\sigma = 6.4$ mJy), and it is not clear how much of the dispersion is due to intrinsic variations or to observational errors caused by the diffuse nature of this source. Object W-3 is associated with an optical, bow-shaped nebulosity (see Lenzen 1988) identified as an HH object (Hartigan & Lada 1985; Hartigan et al. 1986). The association to an optical object suggests that this radio source is likely to be on the near side of the molecular cloud. We suggest that the radio emission from W-3 corresponds to emission from shocked gas excited by a wind that is flowing away from source W-2.

Herbig-Haro objects are not strong emitters at radio wavelengths. HH-1 and HH-2, the first such objects detected in the radio band, have flux densities at 6 cm of ~ 1 mJy, which implies luminosities of $\sim 3 \times 10^{17}$ ergs s^{-1} Hz^{-1}, and flat spectral indices between 20 and 2 cm (Pravdo et al. 1985; Rodríguez et al. 1990). The most luminous HH objects known to date, HH 80–81, have luminosities at 6 cm of ~ 3–6×10^{18} ergs s^{-1} Hz^{-1} (Rodríguez & Reipurth 1989) and spectral indices between 1.5 and 15 GHz of -0.3 (Martí et al. 1993). The nature of the radio emission from HH objects is commonly assumed to be optically thin free-free emission. The excitation mechanism is thought to be shock ionization as a result of the interaction of a stellar wind with dense ambient gas.

The detection of radio emission from objects W-3 and S in Cep A West may be related to their high shock velocities. At the position of the peak emission from W-3 the spectral index is -0.1, consistent with free-free emission. From the observed peak value of the flux density at 4.9 GHz (0.73 mJy beam^{-1}), adopting a shock velocity of $v_o = 476$ km s^{-1} (Hartigan et al. 1986) we find, using equation (4), a preshock density of 2×10^3 cm^{-3}. Similarly, for source S, identified as an HH object with very wide line profiles (full velocity width in the Hα line of 356 km s^{-1}; Hartigan et al. 1986), we find a preshock density of 1×10^3 cm^{-3}. The radio emission from the envelope of W-3 shows, however, negative spectral indices. The nature of this radio emission is probably synchrotron emission from relativistic electrons that are accelerated at the shock front by the diffusive acceleration mechanism.

4.3. *Centers of Activity toward Cep A and Their Driving Sources*

Several indicators have shown beyond doubt that Cep A is an active region of star formation. A high-velocity bipolar molecular outflow, oriented roughly in an east-west direction and centered on Cep A East, was first reported by Rodríguez et al. (1980a). Further observations, with higher sensitivity and angular resolution, revealed a more complex morphology for the outflow, including multiple lobes of emission (Hayashi, Hasegawa, & Kaifu 1988; Bally & Lane 1990). HH objects, often found in the vicinity of newly formed stars associated with molecular outflows, have been seen from two directions, $\sim 2'$ northeast of the Cep A East region (Lenzen 1988) and $\sim 1'$ northwest of the Cep A West region (Hartigan & Lada 1985; Hartigan et al. 1986). In addition, Corcoran, Ray, & Mundt (1993) found several optical HH objects linked in a large ($\sim 3'$) elliptical loop, the major axis of which points roughly in the east-west direction. Finally, H_2O maser emission has been detected from three well-separated centers of activity, each closely associated with a compact radio source (Lada et al. 1981; Cohen et al. 1984). The maser spots are thought to mark the position of young stars in the field.

Less successful, however, has been the identification of the powering source (or sources) of the activity toward Cep A. Polarization measurements of the large-scale IR reflection nebula toward the northeast of Cep A show that the illuminating source is located near the center of the region

containing the compact radio sources. Lenzen, Hoddap, & Solf (1984) found that the lines perpendicular to the polarization vectors converge near source 2 while Joyce & Simon (1986) found a convergence point located between, and within $\sim 1''$ of, the positions of radio sources 3b and 8. Given the large errors in the determination of the centroid position, the identification of a particular radio object as the source of scattered light is, however, uncertain. Lenzen (1988) found that the motions of the HH objects toward the northeast (HH-NE) and west (GGD 37) of the Cep A East region appear to have a common origin, located near the compact radio sources 2 and 3, leading him to suggest that a single object drives all the activity seen toward the Cep A region. Based on the data presented here, we argue that Cep A East and Cep A West correspond to independent centers of activity, each powered by a different source (or sources) of energy.

We believe that the activity within the east region is powered by more than a single object. We propose as driving sources of activity objects 2 and 3d, whose morphologies and dependences of flux density and angular size with frequency imply that they correspond to bipolar, confined jets. Additional support for this hypothesis is provided by their close association to OH and H_2O maser centers of activity (Lada et al. 1981; Cohen et al. 1984; Migenes, Cohen, & Brebner 1992). We previously argued (see § 4.1.2) that the radio emission from the string sources arises from shock-excited gas at the edge of molecular structures, powered by a stellar wind from an external source, and therefore that the string sources do not contain energy sources of their own. The question arises as to what is the powering source of the chain features. We suggest that the northerly (objects 4, 5, 6) and westerly (objects 1a, 1b) radio chains, which are found to be roughly aligned with the jet axis of object 2, are likely to be excited as the confined stellar wind from object 2 impinges on the molecular clouds. In addition, we suggest that the radio emission from the easterly radio chain (objects 7a–7d) might be powered by the wind from object 3d, the major axis of which is approximately aligned in the direction of string 7.

Whether there is one or more than one source driving the complex molecular outflow seen within the Cep A East region is still an open question. Corcoran et al. (1993) suggested that the ellipse of HH emission and the molecular outflow derive from a poorly collimated wind driven by a single source, most likely object 2. However, the observations of Rodríguez et al. (1994), which show that the radio emission from object 2 arises in a biconical, highly collimated, ionized wind in a direction at a P.A. of $44° \pm 4°$, and those of Torrelles et al. (1993), which show it is surrounded by a high-density molecular structure, argue against object 2's being the driving source of a poorly collimated east-west outflow. Observations with high sensitivity and angular resolution by Bally & Lane (1990) show that the outflowing molecular gas centered on Cep A East consists of two *blueshifted-redshifted* pairs of lobes oriented in directions with P.A.'s of $\sim 27°$ and $\sim 101°$. It is interesting to note that these directions are similar to those of the major axes of the jet sources 2 and 3d, respectively. The direction of the elongation of source 3d (P.A. 107°), as well as the orientation of the alignment of its ultracompact components (P.A. 114°), have roughly the same position angle as that of the *east-west* pair of lobes of the large-scale quadrupolar molecular flow (P.A. 101°). Thus, it is possible that the large-scale quadrupolar molecular structure might be produced by the winds from these two outflow sources, rather than being produced by the structure of the environment as suggested by Torrelles et al. (1993).

We do not necessarily attribute all the activity in the Cep A East region to these two sources, however. For instance, it is possible that the loop of HH emission may be associated with a third outflow object. Hughes et al. (1995) suggested that a potential candidate for the energy source of the HH phenomena and the poorly collimated wind is the variable radio source 9, which is located near the apex of the ellipsoidal feature. This object, possibly a pre–main-sequence star, has already been suggested as the driving source of a bullet of ionized gas moving at a speed of 300 km s^{-1} (Hughes 1993). The high degree of outflow activity proposed to take place within the core of the Cep A region is not unusual. Examples of small (<0.1 pc) regions of star formation with multiple outflows include the DG Tau (Mundt & Fried 1983), HH 24 (Jones et al. 1987), and HL Tau/HH 30 (Mundt, Ray, & Bührke 1988) regions.

Finally, we propose that the radio emission from Cep A West, as well as the emission from the GGD 37 HH objects, is powered by the wind from an energy source located within that region (possibly associated with radio component W-2). The colinearity between the radio sources W-2, W-3, and the GGD 37 HH objects, together with the proper motions of the latter, which show that they are expanding away from a point near the radio objects (Lenzen 1988), strongly suggest that the GGD 37 objects correspond to shocked gas at the edge of a cavity excited by the wind starting from source W-2. Interestingly, the western part of the large-scale molecular outflow shows a flow reversal, from redshifted to blueshifted gas, near the position of the HH objects GGD 37. We suggest that the blueshifted gas is closely associated with the GGD 37 objects, which exhibit highly blueshifted emission lines and proper motions along the axis of the flow (Lenzen 1988). These HH objects correspond then to shock-excited gas inside the boundaries of the blueshifted molecular outflow driven by the confined wind from object W-2.

5. SUMMARY

We have made multifrequency radio continuum observations, with matching beams, of the Cep A star-forming region using the VLA. These observations have allowed a detailed determination of the spectral indices of the radio emission from the more than 15 individual radio sources within this region, which have provided important clues about the nature of their radio emission. The main results and conclusions presented in this paper are summarized as follows:

1. Objects 2, 3c, and 3d, located in the central part of the Cep A East region, are characterized by being compact and bright and having positive spectral indices ($\alpha > 0.3$). These characteristics, together with their association with centers of maser activity, suggest that they are excited by centrally contained energy sources.

The flux density and angular size of object 2, the brightest radio source at 15 GHz, show power-law dependence with frequency of the form $\nu^{0.7}$ and $\nu^{-0.6}$, respectively. These dependences are well explained by a model in which the emission is thermal emission arising from a collimated jet of ionized gas, of constant temperature, velocity, and ioniza-

tion fraction, and jet width with a power-law index of 1.2. The major axis of source 2, at a P.A. of 42°, points within a few degrees in the direction of the diffuse sources 1a, 1b, 4, 5, and 6. Object 3d shows dependences of flux density and angular size with frequency of the form $\nu^{0.28}$ and $\nu^{-0.28}$, respectively, suggesting that the radio emission from this source also arises from a collimated, ionized wind. Its major axis, at a P.A. of 107°, appears elongated in the direction of string 7.

2. Objects 3a, 8, and 9, also located in the central part of Cep A East, are characterized by being compact and exhibiting considerable variations in their flux densities. Source 3a is associated with an IR source. Source 8 has a large negative spectral index while source 9 exhibits a flat spectrum. These characteristics suggest that these objects have energy sources of their own, probably low-mass pre–main-sequence stars.

3. The morphology of the radio sources located at the borders of the NH_3 condensations (sources 1a, 1b, 4, 5, 6, 7a, 7b, 7c, 7d) is characterized by showing extended envelopes of diffuse emission and relatively brighter cores. Most of these string sources exhibit a mixture of flat and negative spectral indices across their faces, indicating that both thermal and nonthermal mechanisms are giving rise to the radio emission. Flat indices are usually seen toward the cores while negative indices are seen toward the envelopes, suggesting that the nonthermal emission dominates in the envelopes and/or interclump medium. The spectral indices of the integrated emission from sources 1a, 5, 7b, and 7c are considerably negative ($\alpha \leq -0.4$) while those of sources 1b, 4, 6, and 7a are in the range from -0.3 to -0.1. We suggest that the radio emission from the string sources arises from shock-excited ionized gas at the interface between the confined winds and the molecular clumps. The nonthermal radiation is likely to be the result of the acceleration of a small fraction of the electrons in the bow shocks formed by the interaction of the stellar wind and ambient high-density clumps by the diffusive shock-acceleration mechanism. We find that the nonthermal emission dominates the thermal emission when the density of the thermal electrons is below a critical density of $\sim 5 \times 10^3$ cm^{-3}.

4. We propose that the excitation of the northern chain (composed of objects 4, 5, and 6) and of string 1 (composed of objects 1a and 1b), which are roughly aligned in the direction of the major axis of source 2, is produced by shock waves driven by the confined stellar wind that arises from this object. To simultaneously explain the observed properties of the radio emission from object 2 and from the string sources with flat spectral indices requires the stellar wind to have a mass-loss rate of $2 \times 10^{-6}\ M_\odot$ yr^{-1} and a velocity of 1900 km s^{-1}. In addition, we propose that the excitation of string 7 might be produced as the confined wind from source 3d impinges on the edge of the Cep A-3 NH_3 cloud. The radio emission from the string sources with negative spectral indices can be explained as synchrotron radiation arising in a medium with a magnetic field strength of ~ 0.3 mG and a density of relativistic electrons of $\sim 5 \times 10^{-4}$ cm^{-3}.

5. The radio morphology of the Cep A West source, which shows two compact components toward the southeast and an elongated, diffuse, component toward the northwest, is reminiscent of a champagne or collimated outflow. We find that the spectral index of the peak emission from the extended component (W-3) is -0.1 while that of its integrated emission is -0.4, suggesting that a synchrotron emission component coexists with free-free emission. The spectral index of the peak emission from the brightest compact object (W-2) is 0.6, suggesting it has an energy source of its own. We conclude that the Cep A West region and the associated GGD 37 HH objects constitute an isolated region of activity, powered by an energy source distinct from that powering the Cep A East region.

S. C. acknowledges the support from a Smithsonian Postdoctoral Fellowship. L. F. R. thanks DGAPA, UNAM, and CONACyT, México, for their support. J. M. T. is partially supported by DGICYT grant PB92-0900 and by Junta de Andalucía (Spain). G. G. gratefully acknowledges the support of a Guggenheim Fellowship.

REFERENCES

André, P., Montmerle, T., & Feigelson, E. D. 1987, AJ, 93, 1182
Bally, J., & Lane, A. P. 1990, in ASP. Conf. Proc. 14, Astrophysics with Infrared Arrays, ed. R. Elston (San Francisco: ASP), 273
Blandford, R., & Eichler, D. 1987, Phys. Rep., 154, 1
Blitz, L., & Lada, C. J. 1979, ApJ, 227, 152
Cohen, R. J., Brebner, G. C., & Potter, M. M. 1990, MNRAS, 246, 3P
Cohen, R. J., Rowland, P. R., & Blair, M. M. 1984, MNRAS, 210, 425
Corcoran, D., Ray, T. P., & Mundt, R. 1993, A&A, 279, 206
Crusius-Wätzel, A. R. 1990, ApJ, 361, L49
Curiel, S., Cantó, J., & Rodríguez, L. F. 1987, Rev. Mexicana Astron. Astrofis., 14, 595
Curiel, S., Rodríguez, L. F., Cantó, J., Bohigas, J., Roth, M., & Torrelles, J. M. 1989, Astrophys. Lett. Comm., 27, 299
Curiel, S., Rodríguez, L. F., Moran, J. M., & Cantó, J. 1993, ApJ, 415, 191
Garay, G., Moran, J. M., & Reid, M. J. 1987, ApJ, 314, 535
Gyulbudaghian, A. L., Glushkov, Yu. I., & Denisyuk, E. K. 1978, ApJ, 224, L137
Hartigan, P., & Lada, C. J. 1985, ApJS, 59, 383
Hartigan, P., Lada, C. J., Stocke, J., & Tapia, S. 1986, AJ, 92, 1155
Hayashi, S. S., Hasegawa, T., & Kaifu, N. 1988, ApJ, 332, 354
Henriksen, R. N., Ptuskin, V. S., & Mirabel, I. F. 1991, A&A, 248, 221
Hoare, M. G., & Garrington, S. T. 1995, ApJ, 449, 874
Hughes, V. A. 1985, ApJ, 298, 830
———. 1988, ApJ, 333, 788
———. 1989, AJ, 97, 1114
———. 1991, ApJ, 383, 280
———. 1993, AJ, 105, 331
Hughes, V. A., Cohen, R. J., & Garrington, S. 1995, MNRAS, 272, 469
Hughes, V. A., & Moriarty-Schieven, G. 1990, ApJ, 360, 215
Hughes, V. A., & Wouterloot, J. G. A. 1982, A&A, 106, 171
———. 1984, ApJ, 276, 204
Jones, B. F., Cohen, M., Wehinger, P. A., & Gehren, T. 1987, AJ, 94, 1260
Joyce, R. R., & Simon, T. 1986, AJ, 91, 113
Lada, C. J., Blitz, L., Reid, M. J., & Moran, J. M. 1981, ApJ, 243, 769
Lang, K. R. 1980, Astrophysical Formulae (2d ed.; Berlin: Springer)
Lenzen, R. 1988, A&A, 190, 269
Lenzen, R., Hoddap, K.-W., & Solf, J. 1984, A&A, 137, 202
Martí, J., Rodríguez, L. F., & Reipurth, B. 1993, ApJ, 416, 208
Migenes, V., Cohen, R. J., & Brebner, G. C. 1992, MNRAS, 254, 501
Montmerle, T., & André, P. 1988, in Formation and Evolution of Low Mass Stars, ed. A. K. Dupree & M. T. V. T. Lago (NATO ASI Ser. C, 241) (Dordrecht: Kluwer), 225
Mouschovias, T. C. 1976, ApJ, 207, 141
Mundt, R. 1988, in Formation and Evolution of Low Mass Stars, ed. A. K. Dupree & M. T. V. T. Lago (NATO ASI Ser. C, 241) (Dordrecht: Kluwer), 257
Mundt, R., & Fried, J. W. 1983, ApJ, 274, L83
Mundt, R., Ray, T. P., & Bührke, T. 1988, ApJ, 333, L69
Pravdo, S. H., Rodríguez, L. F., Curiel, S., Cantó, J., Torrelles, J. M., Becker, R. H., & Sellgren, K. 1985, ApJ, 293, L35
Reid, M. J., Argon, A. L., Masson, C. R., Menten, K. M., & Moran, J. M. 1995, ApJ, 443, 238
Reid, M. J., & Moran, J. M. 1981, ARA&A, 19, 231
Reynolds, S. P. 1986, ApJ, 304, 713

Rodríguez, L. F., & Cantó, J. 1983, Rev. Mexicana Astron. Astrofis., 8, 163
Rodríguez, L. F., Curiel, S., Moran, J. M., Mirabel, I. F., Roth, M., & Garay, G. 1989, ApJ, 346, L85
Rodríguez, L. F., Garay, G., Curiel, S., Ramírez, S., Torrelles, J. M., Gómez, Y., & Velázquez, A. 1994, ApJ, 430, L65
Rodríguez, L. F., Ho, P. T. P., & Moran, J. M. 1980a, ApJ, 240, L149
Rodríguez, L. F., Ho, P. T. P., Torrelles, J. M., Curiel, S., & Cantó, J. 1990, ApJ, 352, 645
Rodríguez, L. F., Martí, J., Cantó, J., Moran, J. M., & Curiel, S. 1993, Rev. Mexicana Astron. Astrofis., 25, 23
Rodríguez, L. F., Moran, J. M., Ho, P. T. P., & Gottlieb, E. W. 1980b, ApJ, 235, 845
Rodríguez, L. F., & Reipurth, B. 1989, Rev. Mexicana Astron. Astrofis., 17, 59
Sargent, A. I. 1977, ApJ, 218, 736
Torrelles, J. M., Ho, P. T. P., Rodríguez, L. F., & Cantó, 1985, ApJ, 288, 595
———. 1986, ApJ, 305, 721
Torrelles, J. M., Verdes-Montenegro, L., Ho, P. T. P., Rodríguez, L. F., & Cantó, J. 1993, ApJ, 410, 202
Wouterloot, J. G. A., Habing, H. J., & Herman, J. 1980, A&A, 81, L11
Yusef-Zadeh, F., Cornwell, T. J., Reipurth, B., & Roth, M. 1990, ApJ, 348, L61